Analyst

Accepted Manuscript

ROYAL SOCIETY OF CHEMISTRY

www.rsc.org/analyst

Layer-by-Layer Polyelectrolyte Encapsulation of *Mycoplasma pneumoniae* for Enhanced Raman Detection

Omar E. Rivera-Betancourt[1], Edward S. Sheppard[2], Duncan C. Krause[2], and Richard A. Dluhy[1*]

[1] Department of Chemistry, University of Georgia, Athens, GA 30602

[2] Department of Microbiology, University of Georgia, Athens, GA 30602

*Author to whom correspondence should be sent

tel: +1-706-542-1950

fax: +1-706-542-9454

dluhy@uga.edu

Abstract

Mycoplasma pneumoniae is a major cause of respiratory disease in humans and accounts for as much as 20% of all community-acquired pneumonia. Existing mycoplasma diagnosis is primarily limited by the poor success rate at culturing the bacteria from clinical samples. There is a critical need to develop a new platform for mycoplasma detection that has high sensitivity, specificity, and expediency. Here we report the layer-by-layer (LBL) encapsulation of *M. pneumoniae* cells with Ag nanoparticles in a matrix of the polyelectrolytes poly(allylamine hydrochloride) (PAH) and poly(styrene sulfonate) (PSS). We evaluated nanoparticle encapsulated mycoplasma cells as a platform for the differentiation of *M. pneumoniae* strains using surface enhanced Raman scattering (SERS) combined with multivariate statistical analysis. Three separate *M. pneumoniae* strains (M129, FH and II-3) were studied. Scanning electron microscopy and fluorescence imaging showed that the Ag nanoparticles were incorporated between the oppositely charged polyelectrolyte layers. SERS spectra showed that LBL encapsulation provides excellent spectral reproducibility. Multivariate statistical analysis of the Raman spectra differentiated the three *M. pneumoniae* strains with 97 – 100% specificity and sensitivity, and low (0.1 – 0.4) root mean square error. These results indicated that nanoparticle and polyelectrolyte encapsulation of *M. pneumoniae* is a potentially powerful platform for rapid and sensitive SERS-based bacterial identification.

Introduction

Mycoplasma pneumoniae is a significant human respiratory pathogen, causing bronchitis and atypical or "walking" pneumonia. *M. pneumoniae* accounts for 20% of all community-acquired pneumonia and is the leading cause of pneumonia in older children and young adults[1] [2]. Serologic testing is a common method for diagnosis due to significant challenges posed by direct culture, but suffers from severe limitations, including the need for paired sera obtained at separate physician visits, and thus is impractical for rapid testing.[1] Detection of *M. pneumoniae* by polymerase chain reaction (PCR) yields high specificity, but is prone to false-negatives[3]. The inability to provide rapid and definitive diagnosis delays initiation of appropriate treatment, prolongs morbidity, and increases the likelihood of continued transmission, secondary infections, and long-term sequelae, including chronic lung disease associated with COPD and asthma.[3] Lack of a simple, reliable, rapid diagnostic test is thus a critical barrier to the improved control of *M. pneumoniae*.

Our laboratories have used a combination of surface-enhanced Raman scattering (SERS)-based nanotechnology methods with pattern-recognition approaches to yield direct, rapid, and sensitive detection of infectious agents.[4] Nanofabrication by oblique angle vapor deposition produces Ag nanorods arrays exhibiting extremely high electromagnetic field enhancements.[4-6] Paired with chemometric analysis, this platform can rapidly detect and distinguish with great sensitivity and specificity the Raman spectra of viruses and bacteria, including mycoplasmas.[7-10]

This current study reports on a new SERS platform for mycoplasma detection that is based on modification of Ag nanoparticles (AgNP) to increase their affinity for the bacteria. The direct placement of Ag nanoparticles onto living cells can affect the viability of cells either during the

process of deposition of nanoparticles or shortly after. Therefore, we have adapted the use of layer-by-layer (LBL) encapsulation techniques, which are widely used for modification of substrates such as planar surfaces and nanoparticles.[11-13]

The LBL technique utilizes the consecutive deposition of oppositely charged polyelectrolytes onto surfaces,[14] allowing consecutive layers to be formed.[15-17] A general outline of the LBL assembly procedure begins with a polycation such as poly(allylamine hydrochloride) (PAH), followed with a polyanion such as poly(styrene sulfonate) (PSS). The LBL process is repeated until the planned shell architecture is realized. Biological cells are suitable templates for LBL coatings because they can be used as cores for the development of polyelectrolyte microcapsules while their biological activity is preserved. LBL deposition of polyelectrolyte assemblies affords nanoscale control over the construction of multilayers with charged nanoparticles.[18, 19]

Many microbial and human cells are negatively charged.[20] Polyelectrolyte assemblies can thus facilitate adhesion of nanoparticles to cells and provide stability to the sandwich-like polyelectrolyte/nanoparticle coating. The use of electrostatic LBL encapsulation of bacterial cells with SERS-active nanoparticles has previously been explored by several research groups,[20-24] and has recently been reviewed.[20] Layer-by-layer polyelectrolyte assembly with colloidal Au and Ag nanoparticles has been demonstrated with fungi[21] and bacteria.[24] In this study we used LBL techniques to encapsulate three different strains of *M. pneumoniae* with Ag nanoparticles (AgNPs) for SERS analysis. Our hypothesis is that the charged polyelectrolyte layers should increase the number of contact points between the AgNPs nanoparticles and the bacterial cell for improved SERS spectral quality, thereby increasing accuracy in identification and differentiation of different mycoplasma strains.

Our laboratories have previously used planar Ag nanorod array substrates to detect and differentiate *M. pneumoniae* strains with statistically significant sensitivity and specificity.[9] The current work uses LBL encapsulation as an alternative SERS preparation method to avoid issues with pleomorphism and lysis due to the absence of a cell wall in mycoplasmas. LBL-SERS methods have not previously been reported for detection and identification of mycoplasmas. We used *M. pneumoniae* wild-type strain M129 as a model organism to illustrate the LBL encapsulation procedure. The results presented in this study showed that the LBL method identified three *M. pneumoniae* strains with 97 – 100% specificity and sensitivity, and with extremely low root-mean-square errors.

Materials and Methods

Chemicals. Poly(allylamine hydrochloride) (PAH, M_w ~15,000), sodium (polystyrene sulfonate) (PSS, M_w ~70,000), fluorescein-isothiocyanate-PAH (FITC-PAH, M_w ~15 kDa), and 4′,6-diamidino-2-phenylindole dihydrochloride (DAPI) were purchased from Sigma-Aldrich (St. Louis, MO). PELCO® NanoXact™ citrate-capped Ag colloid nanoparticles (50 nm) were purchased from Ted Pella, Inc., (Redding, CA). Non-functionalized (SiOH) silica microspheres (600 nm) were purchased from Bangs Laboratories, Inc., (Fishers, IN).

Culture and Preparation of Bacterial Strains. Two major wild-type *M. pneumoniae* subtypes, M129 and FH,[25] as well as strain II-3, a spontaneously arising avirulent mutant derived from M129,[26, 27] were used in this study. Mycoplasmas were grown to log phase with a 1 µl/ml inoculation. The wild-type and mutant strains were grown in 25 ml of SP4 medium[28, 29] in cell culture flasks at 37˚C for 72-96 h and harvested when the phenol red pH indicator turned orange (pH approx. 6.5). The growth medium for the M129 and FH strains was poured off and the cells were scraped from the flask surface into 2.5 ml of fresh SP4 medium. For the II-3 strain, which fails to attach to plastic, cell suspensions were collected through centrifugation at 25,000×g for 25 min at 4˚C and then suspended in 2.5 ml of fresh SP4. Mycoplasma suspensions were syringe-passaged 10 times with a 25-gauge needle to disperse the cells, and aliquots of each were serially diluted for plating to measure colony-forming units (CFU). A 500 µl aliquot of each strain was transferred to a separate tube and fixed in SP4 by adding 500 µl of 8% formaldehyde (pH 7.0-7.5) for a final 4% formaldehyde concentration and stored at 4˚C until used for cell encapsulation.

Polyelectrolyte Encapsulation. A three-step wet chemical assembly process was used for encapsulation of the mycoplasma cells.

Step 1. Mycoplasma Phase. The first step involved encapsulating the bacterial cells in a layer-by-layer fashion by alternating depositions of PAH/PSS/PAH. Polyelectrolyte solutions were dissolved in 0.5M NaCl at the concentration of 1 mg/ml. The procedure began by coating with PAH; 500 µl of the cell suspension was combined with 250 µl of 1 mg/ml PAH and 250 µl of 1 mg/ml PSS and mixed for 15 min at room temperature. This mixture was centrifuged for 10 min at 17,000 rpm at 4˚C, excess polyelectrolyte solution was discarded, and the cells suspended and washed two additional times with cold ultrapure water. The cell suspension was centrifuged for 10 min at 17,000 rpm at 4˚C after each wash. To the same tube were added 250 µl of 1 mg/ml solution of PAH, and cold water to a final volume of 1 ml. The suspension was mixed for 15 min, and then centrifuged for 10 min at 17,000 rpm at 4˚C. Excess polyelectrolyte solution was discarded and the cells suspended and washed two times with cold ultrapure water. The supernatant was discarded at this point leaving the pelleted cells.

Step 2. AgNP Phase. The second step involved coating the AgNP colloidal suspension with PAH and PSS. 1 ml of the Ag col loid suspension was centrifuged at 7000 rpm for 10 min at 4˚C. The supernatant was discarded and an additional 900 µl of colloidal suspension was added. To this AgNP suspension was added 50 µl of 1 mg/ml PAH and the contents mixed for 15 min. Then 50 µl of 1 mg/ml PSS were added and the contents again mixed for 15 min. The suspension was then centrifuged for 10 min at 17,000 rpm at 4˚C. Excess polyelectrolyte solution was discarded and the AgNP's suspended and washed two times with cold ultrapure water.

Step 3. Encapsulation of Cells. The encapsulated mycoplasma pellet from Step 1 was mixed with the polyelectrolyte-coated AgNPs from Step 2 for 15 min and then centrifuged for 10 min at 17,000 rpm at 4˚C. The supernatant was discarded and the pellet suspended and washed twice with cold ultrapure water, centrifuging for 10 min at 17,000 rpm after each wash. At the end of the process, the cells were suspended in water.

Characterization of the Encapsulated Cells. The uniformity of the LBL polyelectrolyte coating was investigated using FITC-PAH and DAPI nucleic acid stains. A Nikon A1R confocal microscope with a CFI Plan APO VC 60× oil immersion objective with NA=1.4 and 0.13 mm working distance was used to image the *M. pneumoniae* cells. Scanning electron microscopy (SEM) images of the uncoated bacteria were obtained using a Zeiss (Jena, Germany) 1450EP SEM. For the encapsulated cells, images were obtained using an FEI (Hillsboro, OR) Inspect F FEG-SEM. Samples for SEM were fixed as described elsewhere,[30] with modifications. Samples of cells were prepared by dispersing 100 μL of a cellular suspension on the surface of a glass coverslip pre-coated with poly-L-lysine and incubated overnight at 37˚C. The samples were fixed in 2% glutaraldehyde in Na cacodylate buffer for one hour and then washed twice in Na cacodylate buffer for 5 min each. The samples were post-fixed in 1% OsO_4 in Na cacodylate buffer for one hour, washed once afterwards with Na cacodylate buffer for 10 minutes, and then rinsed with water twice for 5 min. The SEM coverslips were treated with a sequential ethanol dehydration series (5 min each step) with 25, 50, 75, 85, 95, and 3× 100% washes, critical point dried, and sputter coated with Au for examination.

SERS Measurements of the M. pneumoniae Strains. SERS spectra were acquired using a Renishaw (Hoffman Estates, IL) inVia confocal Raman microscope system using a 785 nm near-

IR diode laser as the excitation source. Radiation from the diode laser was attenuated to <15 mW using a series of neutral density filters and focused onto the sample using a 20× microscope objective. Spectra were collected between 1800 – 400 cm^{-1} and integrated for 30s per scan with 1 scan per spectrum. The SERS spectra of the encapsulated cells with polyelectrolytes and AgNP were collected applying a 10 µl sample droplet to a copper foil substrate that was cleaned thoroughly with copious amounts of methanol and acetone. The drop was dried in an incubator at 75˚C and then rinsed thoroughly with ultrapure water and dried under a stream of N_2 prior to analysis. A minimum of ten spectra were collected for each bacterial strain from different locations on each individual substrate. Duplicate samples of the LBL-AgNP assemblies for each *M. pneumoniae* strain were prepared to test for reproducibility of the method.

Multivariate Statistical Analysis. Raman spectra were imported into GRAMS AI (Version 8.0 Thermo Electron Corp, Waltham, MA) for spectral averaging and baseline correction. Chemometric analysis was carried out with MATLAB version 7.2 (The Mathworks, Inc., Natick, MA), using PLS Toolbox version 7.0 (Eigenvector Research Inc., Wenatchee, WA). SERS spectra in the range 1650 – 700 cm^{-1} were used for classification. Prior to analysis, first derivatives of the SERS spectra were calculated using the Savitzky-Golay method with a 2^{nd} order polynomial and a fifteen-point window. Each data set was then vector normalized and mean centered. Multivariate statistical analysis of the mycoplasma spectra was performed using principal components analysis (PCA), hierarchical cluster analysis (HCA), and partial least squares discriminant analysis (PLS-DA) using the PLS Toolbox software. The calculated principal components were used as inputs to the HCA algorithm, which used the Ward's method algorithm to evaluate minimum variances between clusters.

Results and Discussion

Characterization of LBL Encapsulated Mycoplasma. We used *M. pneumoniae* wild-type strain M129 as a model organism to illustrate the LBL encapsulation procedure. Synthetic polycation/polyanion pairs, *i.e*. PAH/PSS, were used to produce layered shells that covered the bacteria. PAH was deposited as the first layer to balance the negative surface charge of the mycoplasma cells, followed by the polyanion PSS, and then a final layer of PAH was added. Therefore, the final mycoplasma LBL structure was PAH/PPS/PAH.

PAH was also used as the first polyelectrolyte layer on the citrate-reduced AgNPs, followed by a layer of PSS. This final polyanion layer provides higher stability to the structure, as well as sensitivity to temperature and permeability.[12, 17, 20] Figure 1 shows a schematic representation of the deposition process. The bacteria were treated with PAH/PPS/PAH rather than just one layer of PAH since the three-layer system dramatically increased the quality of the resulting SERS spectra of the encapsulated cells. Additional layers of polyelectrolytes also increases the electrostatic interaction of the bacteria with the Ag nanoparticles, as well as the number of contact points between the nanoparticles and bacterial surface.

The cells were washed after every LBL deposition cycle to remove any excess polyelectrolytes. Deposition of the polyelectrolyte-coated AgNPs on the mycoplasma cells could be monitored visually. Originally, the cell suspensions were clear; however, the suspended cells acquired a brownish-yellow color during the deposition of the AgNPs. The color of the suspension was due to the presence of the bound AgNPs in the LBL matrix and not to free, unbound nanoparticles, as these were removed during the washing steps. The final washing steps resulted in a clear supernatant, indicating no AgNPs were being released from the cell suspensions.

Cell morphology of wild-type *M. pneumoniae* M129 wild type and mutant II-3 was directly characterized by SEM, as previously described.[30] Mycoplasmas have a marked tendency toward pleomorphism due to the absence of a cell wall.[31, 32] Therefore, the use of an electron source for high-resolution imaging can be a challenge. We employed two different SEM's for this work. The first was an environmental SEM (ESEM). This technique is commonly employed for the detection of different living organisms on a "wet" and/or uncoated state.[33] ESEM micrographs of the uncoated, wild-type M129 cells are shown in Figs. 2A and 2B. The cells in these images appeared elongated with a well-defined, tapered tip structure and long, filamentous tail; their size was approximately 1-2 μm in length and 0.1-0.2 μm in width. While the predominant morphological forms present in the ESEM micrographs observed were elongated, minor amounts of ovoid and pleomorphic forms were also seen (data not shown).

The polyelectrolyte-encapsulated cells were characterized by field emission SEM (FE-SEM), as seen in Figs. 2C and 2D. In comparison to the smooth surfaces of the uncoated cells in Fig. 2A and Fig. 2B, the encapsulated mycoplasmas in Figs. 2C and 2D showed large aggregates and roughened features. The Ag nanoparticles that we used in this work were ~50 nm in diameter; however, the extent of aggregation seen in Fig. 2 makes it is difficult to determine the size and location of the Ag nanoparticle complexes within the LBL-mycoplasma structures. Aggregation has previously been reported in LBL polyelectrolyte encapsulation of other bacterial species, with the extent of aggregation depending on the fixation protocols as well as the bacterial cell surface biochemistry.[24]

The presence of the polyelectrolyte-encapsulated AgNPs enhances the aggregation of the mycoplasma cells into clusters. The chemical natures of the polyelectrolytes, as well as the

solution ionic strength, have a strong influence on the polyion complexes that are formed. [17, 34-36] In the current case, we employed a weak polycation (PAH) at relatively low ionic strength (0.5M NaCl) that led to a heterogenous surface topography previously noted as characteristic for PAH/PSS polyelectrolyte systems.[35, 37]

We also conducted fluorescence labeling experiments to confirm the co-localization of the AgNPs on the polyelectrolyte-encapsulated mycoplasmas. These images are shown in Fig. 3. Two different stains were used for this procedure. First, a commonly used nucleic acid dye, DAPI, was used to stain the nucleoid of mycoplasma cells.[38, 39] DAPI is a blue fluorescent nucleic acid stain that preferentially stains A-T complexes in double-stranded DNA (dsDNA).[38, 39] This is illustrated in Fig. 3A, in which the blue images mark the presence of likely individual un-encapsulated *M. pneumoniae* M129 cells stained with DAPI. Figure 3B shows the DAPI image of the mycoplasma after encapsulation with the PAH/PSS polyelectrolytes and AgNPs, and clearly shows the encapsulated bacteria more aggregated than the uncoated bacteria in Fig. 3A.

In conjunction with the DAPI stain, FITC labeled PAH was used to determine whether the PAH/PSS/PAH polyelectrolyte layers and the PAH/PSS coated AgNPs were bound to the encapsulated mycoplasmas.[40] Figure 3C shows the green fluorescence emission of FITC-PAH incorporated into the PAH/PSS/PAH layers on *M. pneumoniae* M129 for the same field as Fig. 3B. A comparison of Fig. 3B (DAPI-stained mycoplasma emission) with Fig. 3C (FITC-PAH emission) showed significant fluorescence overlap between the two images, consistent with co-localization of the polyelectrolytes with the bacteria. Figure 3D is a merged image of DAPI-labeled *M. pneumoniae* (blue) after deposition of the FITC-PAH layers (green). This image was taken at a different location than those of Fig. 3B and Fig. 3C. Figure 3D shows that not all of

the FITC signal is associated with the DAPI signal. This suggests that some of the polyelectrolyte may be interacting with sample components other than whole mycoplasma bacterial cells. The additional bacterial components in Figure 3 may be due to cellular debris, as mycoplasma does not contain a cell wall, and cell lysis potentially occurs.[32]

Figure 3 illustrates the principle that while the areas of polyelectrolyte coverage were not uniform,[41] the labeled PAH predominately co-localized with the bacteria. In addition, the encapsulated AgNP nanoparticle distribution was similar to that of the polyelectrolytes.

SERS Spectra of the M. pneumoniae Strains. The Raman spectra of bacteria reflect predominantly phenotypic information arising from proteins, nucleic acids, lipids, carbohydrates and endogenous biomolecules.[42, 43] In order to detect and identify pathogens of interest, it is necessary to ensure that the observed Raman bands are specific to the targeted organisms but not to the overall environment, i.e., the media or solvents. The mycoplasma SP4 growth medium is removed from the sample prior to spectral analysis; therefore, it was not included in the background analysis. Instead, the background control used in these samples was from the last part of the LBL assembly process that includes both polyelectrolytes as well as the AgNPs, *i.e.*, the silver nanoparticle-polyelectrolyte layer Ag/PAH/PSS.

We also incorporated a second negative control sample in these experiments. This negative control utilized non-functionalized silica microspheres (SiMS) of 600 nm diameter. The size of these microspheres closely resembles the actual size of a mycoplasma bacterium cell, ~1000 nm. These experiments used the silica microspheres as a sacrificial or electroactive core to simulate the bacterium as a negative control . We performed all the experimental protocols using the SiMS in place of the bacteria. Therefore, these Si microsphere were coated with PAH and PSS

and functionalized with Ag nanospheres, resulting in a LBL structure of SiMS/PAH/PSS/PAH/Ag/PAH/PSS. For brevity, this will be referred to as the SiMS negative control in the remainder of the article.

Figure 4 illustrates the reproducibility of the SERS spectra obtained from mycoplasmas prepared using this LBL encapsulation process. Samples containing M129/PAH/PSS/PAH/Ag/PAH/PSS were prepared as described above, and then spot dried on a piece of copper foil. Spectra of the dried samples were obtained from 10 different locations. The SERS experiments were repeated several times with a newly prepared sample each time. The same approach was used when acquiring the SERS spectra of the other two *M. pneumoniae* strains, as well as the Ag/PAH/PSS background and the SiMS negative controls. The spectra in Fig. 4 were the raw, unprocessed, and baseline un-corrected spectra of the M129 mycoplasma strain. The overlaid spectra demonstrate the reproducibility of the LBL encapsulation process.

SERS is highly dependent on, and sensitive to, the proximity of the AgNPs to the cell surface. Functional groups such as COO^- and NH_2^+ may define the modes of interaction between the bacterial surface and the AgNPs.[22, 44-46] Figure 5 illustrates the average SERS spectra in the 1800 – 400 cm^{-1} range of the three *M. pneumoniae* strains, the Ag/PAH/PSS background and the SiMS negative control . For each sample, including the controls, ten spectra were taken at each of two different spots, baseline-corrected, and normalized for visualization. The Raman vibrations at 1504, 1459, 1277, 1130 and 1080 cm^{-1} were found in all spectra, although their intensities varied.[47] The spectra of the different strains did exhibit some differences; for example, the bands at 1580 and 1299 cm^{-1} were characteristic for *M. pneumoniae* M129, while the bands at 1383, 1359 and 668 cm^{-1} were characteristic for *M. pneumoniae* FH and II-3. The most significant spectral differences occurred in the 1000 – 400 cm^{-1} region. To improve the resolution of

overlapping bands and eliminate potential artifacts induced by baseline correction, we also compared first derivative spectra of these samples, as seen in Fig. 6. A list of the observed Raman vibrations attributed to the mycoplasma strains in Figs. 5 and 6 as well as their tentative assignments are found in Table 1. Detailed spectral band assignments have been published elsewhere.[22, 24, 44, 45, 47-49]

Classification of the M. pneumoniae Strains. The excellent spot-to-spot and sample-to-sample reproducibility of the SERS Raman spectra offered by the LBL methods allows for multivariate analysis as a method for classification and identification. The statistical basis for the application of chemometric techniques to vibrational spectroscopy is well established.[50] Spectral interpretation can be accompanied by unsupervised pattern recognition methods such as principal component analysis (PCA)[46] and hierarchical cluster analysis (HCA), as well as supervised methods such as partial least squares discrimination analysis (PLS-DA).[4, 51, 52]

We have previously used chemometric methods to analyze nanorod-array SERS spectra of human and avian mycoplasma species extracted into a water-formalin mixture for inactivation of the bacteria, a process that potentially lyses the cells.[9, 53] The current work is the first to use the LBL method to ensure preparation of whole, intact encapsulated mycoplasma cells for use in SERS classification studies. The high quality and reproducibility of the LBL SERS spectra, as seen in Figs. 4 – 6, demonstrate that these spectra are suitable for use in subsequent multivariate statistical processing steps.

The statistical methods PCA, HCA, and PLS-DA were used to determine whether it is possible to discriminate between these three different mycoplasma strains and controls based solely on their LBL SERS spectra. PCA reduces dataset dimensionality by calculating orthogonal

eigenvector projections, and facilitates establishing patterns and grouping of similar spectra.[6, 44, 54] Principal components were calculated from the SERS spectra of the two *M. pneumoniae* M129 and FH wild-type strain, the mutant II-3 strain, a control sample consisting of Ag/PAH/PSS background and the SiMS negative control sample. The PC model consisted of 50 raw spectra, 10 spectra for each *M. pneumoniae* strain and the controls, and was calculated using LBL SERS spectra in the 1650 – 700 cm^{-1} range. As shown in Fig. 7, comparison of the processed spectra using principal components 1 and 2 couldn't clearly differentiate between the three mycoplasma strains and the control Ag/PAH/PSS sample into individual groups. But this PC plot easily tell separates the bacterial samples and background from the SiMS negative control.

In addition, a hierarchical cluster analysis of the LBL SERS spectra was calculated using their principal components. The resulting dendrogram, calculated using the Ward's linkage method (Fig. 8), shows that the three mycoplasma strains, the Ag nanoparticle background, and the SiMS negative control form clearly differentiated clusters.

In addition to the unsupervised PCA and HCA methods, we used PLS-DA to quantitatively determine statistically significant differences among the strains. PLS-DA, unlike HCA and PCA, is a full spectrum, multivariate, supervised method whereby prior knowledge of the classes is used to yield more robust differentiation, minimizing class variation while emphasizing latent variables between or among classes.[55, 56]

Figure 9 presents the results of a PLS-DA analysis of the mycoplasma strains. The model was generated using 50 spectra (10 each for the mycoplasma strains, Ag/PAH/PSS background, and SiMS negative control). The horizontal red line in each panel in Fig. 9 is a calculation of a threshold value of prediction for each modeled class. Spectra with predicted values above the

threshold level are determined to belong to a particular class, while spectra with the predicted values below are excluded. Each panel corresponds to the predictions made for the Ag/PAH/PSS background (Fig. 9A), the SiMS negative control (Fig. 9B), M129 wild-type (Fig. 9C), FH wild-type (Fig. 9D), and II-3 mutant (Fig. 9E). This analysis used 4 latent variables that captured 85.09% of the total variance, followed by cross-validation using Venetian blinds with 7 splits. It is clear from all the panels that PLS-DA was able to classify each spectrum in its class with 100% accuracy. Table 2 provides the statistics calculated from the PLS-DA model, with a root-mean square error after cross-validation (RMSECV) of 0.05 – 0.1 for all classes. This is remarkable classification sensitivity, considering that both M129 and FH are pathogenic wild type strains.

The ability of LBL SERS to accurately differentiate *M. pneumoniae* strains M129 and FH into separate classes may be due to the spectral differences in expressed surface proteins.[9, 30] The high discriminatory ability of LBL SERS seen in this study is similar to that seen when using Ag nanorod-based SERS methods to analyze the spectra of human and avian mycoplasmas, albeit with lower root mean square errors.[9, 53]

Conclusions

M. pneumoniae is a respiratory pathogen that accounts for widespread bronchitis and pneumonia. Unfortunately, the complexity of laboratory culture complicates diagnostic strategies. Currently, the lack of a simple, rapid, clinical diagnostic test delays initiation of appropriate treatment, and increases the risk of continued transmission and long-term sequelae. The purpose of this research was to determine whether charged polyelectrolyte layers could increase the number of contact points between the AgNPs nanoparticles and the bacterial cell for improved SERS spectral quality, thereby increasing accuracy in identification and differentiation of different mycoplasma strains.

In this study, *M. pneumoniae* whole cells were encapsulated layer-by-layer with polyelectrolyte thin films incorporating Ag nanoparticles (Fig. 1). Three strains of *M. pneumoniae* were used as model organisms to illustrate the effectiveness of the LBL encapsulation procedure. The encapsulated bacteria were investigated using both SEM and fluorescence microscopy techniques. SEM images (Figs. 2A and 2B) of the uncoated bacteria showed the expected elongated morphology for mycoplasma, while LBL encapsulation resulted in significant aggregation of the mycoplasma cells into multicellular clusters (Figs. 2C and 2D). Fluorescence microscopy using both a mycoplasma-specific dye (Figs. 3A and 3B) as well as a dye-labeled polyelectrolyte (Figs. 3C and 3D) showed that the polyelectrolytes co-localized with the bacteria, although the areas of polyelectrolyte coverage were not uniform. This behavior is not unexpected for this bacterium, which demonstrates a tendency to clump and aggregate in both clinical isolates and laboratory cultures.[57]

SERS spectra of the LBL encapsulated *M. pneumoniae* strains showed a high degree of reproducibility with good signal-to-noise, making detailed spectral band assignments possible (Figs. 4-6 and Table 1). Unsupervised methods of multivariate statistical analysis, including PCA (Fig. 7) and HCA (Fig. 8), showed a high degree of qualitative class discrimination based on principle components calculated from the SERS spectra. The model-dependent method PLS-DA (Fig. 9 and Table 2) provided quantitative statistical measurements of the sensitivity and specificity of the LBL encapsulation method for discrimination between the three *M. pneumoniae* strains, background, and negative control. In this case, both sensitivity and specificity were between 97 – 100% for all classes modeled, with a low (0.1 – 0.4) root mean square error.

This study demonstrated that LBL polyelectrolyte encapsulation combined with Ag nanoparticle SERS provides a promising platform for accurate identification and differentiation of *M. pneumoniae* strains. The advantage of the LBL method is that charged polyelectrolyte layers should increase the number of contact points between the AgNPs nanoparticles and the bacterial cell for improved SERS spectral quality. In the case of mycoplasma, the use of LBL encapsulation also solves the problem of cell lysis that may complicate spectral analysis.[9] The technique also shows promise for adaptation to sample preparation of *M. pneumoniae* infections in clinical specimens.

Acknowledgements

The research described here was supported by the U.S. Public Health Service through NIH Grants AI096364 and GM102546.

Table1. Raman bands appearing in the LBL SERS spectra of *M. pneumoniae* strains.

Raman Shift, cm^{-1}			Vibrational Band Assignment
M129	FH	II-3	
1606	1606		Phenylalanine
1580			Guanine, Adenine (ring stretch)
1504	1504	1504	C-O-H bend; $(CH_2)_n$ in-phase twist
1459	1459	1459	$\delta(C\text{-}H_2)$ sci.; CH_3 antisym. bend
		1435	$\delta(C\text{-}H_2)$ sci
1396	1396	1396	C-O-H bend; (CH_2 in-phase twist
	1383	1383	C-H def
	1359	1359	C-H def
1299			Amide III
1277	1277	1277	C-O-H bend, Amide III
1247	1247		ν_{as}(COC); δ(CH),Amide III
1204	1200		$C\text{-}C_6H_5$ str., Phe,Trp
1193		1193	δ (C-H), Tyr
		1149	NH_3^+def Pro
1130	1130		C-N and C-C stretch
1080	1080	1080	C-O stretch,
1039	1039		C-H in plane, Phe, C-N Gly
1008	1008	1008	phenylalanine
		969	C-C str
		898	COC str
858	858	859	"buried" tyrosine
		831	"exposed" Tyrosine
	792		Cytosine, uracil (str, ring); CH_2 in-phase rock
785		785	Cytosine, Uracil
738	738	738	Adenosine
712	712	712	Adenine, COO^- def
	668	668	Guanine
	618		Phenylalanine (skeletal)

Table 2. Discrimination results from PLS-DA analysis of the LBL SERS spectra of three *M. pneumoniae* strains, including a control sample (Ag/PAH/PSS).

Modeled Class[a,b]	Sensitivity[d] (CV)	Specificity (CV)	Class Error[e] (CV)	RMSECV[f]
Control[c]	1.000	1.000	0.000	0.123
Negative Ctrl[g]	1.000	1.000	0.000	0.428
M129	1.000	0.975	0.012	0.151
FH	1.000	0.975	0.012	0.104
II-3	1.000	1.000	0.000	0.113

[a] Fifty total spectra were used, 10 for each modeled class. Before calculation, spectra were pre-processed by calculating 1st derivatives, followed by vector normalization and mean centering.

[b] Four latent variables, accounting for 85.09% of the captured variance, were used in this model.

[c] Background sample consisted of Ag nanoparticles derivatized with PAH and PSS layers.

[d] CV, cross-validation based on Venetian blinds method with 7 splits.

[e] Class Error, classification error after cross-validation.

[f] RMSECV, root-mean square error after cross-validation.

[g] Negative control sample consisted of silica microspheres coated with PAH and PSS, and modified with polymer-derivatized Ag nanoparticles..

Figure Captions

Figure 1. Schematic illustration of the encapsulation of the *M. pneumoniae* whole cells into the polyelectrolyte shells containing silver nanoparticles.

Figure 2. SEM images of: *M. pneumoniae* (A) M129 uncoated whole cells, scale bar equals 2 μm; (B) M129 uncoated whole cells at higher magnification, scale bar equals 1 μm; (C) M129/PAH/PSS/PAH/Ag/PAH/PSS cell aggregates, scale bar equals 5 μm; and (D) M129/PAH/PSS/PAH/Ag/PAH/PSS cell aggregates at higher magnification, scale bar equals 3 μm.

Figure 3. Fluorescence microscopy image of: (A) *M. pneumoniae* M129 cells, scale bar equals 1 μm; (B) LBL array of DAPI-M129, scale bar equals 1 μm; (C) LBL array of FITC-PAH on M129 cells, scale bar equals 1 μm; and (D) overlaid image of FITC-PAH coated and DAPI-stained *M. pneumoniae* M129 cells, scale bar equals 6 μm.

Figure 4. Representative SERS spectra of *M. pneumoniae* M129 showing the reproducibility of the spectra collected in ten random locations. Spectra presented here are the original spectra as collected, without further processing.

Figure 5. Representative SERS spectra for (A) the background sample Ag/PAH/PSS, (B) the negative control sample SiMS/PAH/PSS/PAH/Ag/PAH/PSS and the *M. pneumoniae* strains: (C) M129, (D) FH and, (E) II-3. Each is an average of 10 spectra obtained per sample. The spectra have been baseline corrected and normalized for visualization.

Figure 6. First derivative spectra for (A) the background sample Ag/PAH/PSS, B) the negative control sample SiMS/PAH/PSS/PAH/Ag/PAH/PSS and the *M. pneumoniae* strains: (C) M129, (D) FH and, (E) II-3.

Figure 7. PCA scores plot corresponding to: the background sample Ag/PAH/PSS (⓿), the negative control SiMS/PAH/PSS/PAH/Ag/PAH/PSS(*), and *M. pneumoniae* strains FH (⑤), M129 (+), and II-3 (◇) The PC model was constructed from the SERS spectra of the corresponding species using the spectral range 1650-700 cm^{-1}.

Figure 8. A hierarchical cluster analysis dendrogram derived from the PC scores of the *M. pneumonie* species and controls. The nodes group into five recognized clusters and are labeled according to the samples: (A) negative control SiMS/PAH/PSS/PAH/Ag/PAH/PSS; *M pneumonia* strains: (B) II-3; (C) M129; (D) FH; and (E) background sample Ag/PAH/PSS.

Figure 9. PLS-DA cross-validated prediction plot based on the LBL SERS spectra of the *M. pneumoniae* strains. Horizontal red line denotes calculated class prediction threshold level. Predictions for: (A) background sample Ag/PAH/PSS (⓿); (B) negative control SiMS/PAH/PSS/PAH/Ag/PAH/PSS (⊠); and *M. pneumoniae* strains: (C) FH;(⑤); (D) M129 (+); and; (E) II-3 (◇). Fifty spectra, corresponding to 10 spectra in each sample category, are represented in this plot.

References

1. K. B. Waites and D. F. Talkington, *Clin Microbiol Rev*, 2004, **17**, 697-+.
2. K. B. Waitest, M. F. Balish and T. P. Atkinson, *Future Microbiol*, 2008, **3**, 635-648.
3. T. P. Atkinson, M. F. Balish and K. B. Waites, *Fems Microbiol Rev*, 2008, **32**, 956-973.
4. J. D. Driskell, S. Shanmukh, Y. J. Liu, S. Hennigan, L. Jones, Y. P. Zhao, R. A. Dluhy, D. C. Krause and R. A. Tripp, *Ieee Sens J*, 2008, **8**, 863-870.
5. J. D. Driskell, S. Shanmukh, Y. Liu, S. B. Chaney, X. J. Tang, Y. P. Zhao and R. A. Dluhy, *J Phys Chem C*, 2008, **112**, 895-901.
6. S. Shanmukh, L. Jones, Y. P. Zhao, J. D. Driskell, R. A. Tripp and R. A. Dluhy, *Anal Bioanal Chem*, 2008, **390**, 1551-1555.
7. S. Shanmukh, L. Jones, J. Driskell, Y. P. Zhao, R. Dluhy and R. A. Tripp, *Nano Lett*, 2006, **6**, 2630-2636.
8. V. Hoang, R. A. Tripp, P. Rota and R. A. Dluhy, *Analyst*, 2010, **135**, 3103-3109.
9. S. L. Hennigan, J. D. Driskell, R. A. Dluhy, Y. P. Zhao, R. A. Tripp, K. B. Waites and D. C. Krause, *Plos One*, 2010, **5**.
10. P. Negri and R. A. Dluhy, *J Biophotonics*, 2013, **6**, 20-35.
11. W. F. Dong, G. B. Sukhorukov and H. Mohwald, *Phys Chem Chem Phys*, 2003, **5**, 3003-3012.
12. X. G. Hu, W. L. Cheng, T. Wang, Y. L. Wang, E. K. Wang and S. J. Dong, *J Phys Chem B*, 2005, **109**, 19385-19389.
13. R. F. Fakhrullin and R. T. Minullina, *Langmuir*, 2009, **25**, 6617-6621.
14. M. M. de Villiers, D. P. Otto, S. J. Strydom and Y. M. Lvov, *Adv Drug Deliver Rev*, 2011, **63**, 701-715.
15. G. Decher and J. D. Hong, *Makromol Chem-M Symp*, 1991, **46**, 321-327.
16. A. Diaspro, D. Silvano, S. Krol, O. Cavalleri and A. Gliozzi, *Langmuir*, 2002, **18**, 5047-5050.
17. H. Ai, S. A. Jones and Y. M. Lvov, *Cell Biochem Biophys*, 2003, **39**, 23-43.
18. Y. J. Liu, Y. X. Wang and R. O. Claus, *Chem Phys Lett*, 1998, **298**, 315-319.
19. N. E. Cant, H. L. Zhang, K. Critchley, T. A. Mykhalyk, G. R. Davies and S. D. Evans, *J Phys Chem B*, 2003, **107**, 13557-13562.
20. R. F. Fakhrullin and Y. M. Lvov, *Acs Nano*, 2012, **6**, 4557-4564.
21. R. F. Fakhrullin, A. I. Zamaleeva, M. V. Morozov, D. I. Tazetdinova, F. K. Alimova, A. K. Hilmutdinov, R. I. Zhdanov, M. Kahraman and M. Culha, *Langmuir*, 2009, **25**, 4628-4634.
22. M. Kahraman, M. M. Yazici, F. Sahin and M. Culha, *J Biomed Opt*, 2007, **12**.
23. H. B. Zhou, D. T. Yang, N. P. Ivleva, N. E. Mircescu, R. Niessner and C. Haisch, *Anal Chem*, 2014, **86**, 1525-1533.
24. M. Kahraman, A. I. Zamaleeva, R. F. Fakhrullin and M. Culha, *Anal Bioanal Chem*, 2009, **395**, 2559-2567.
25. T. Kenri, N. Okazaki, T. Yamazaki, M. Narita, K. Izumikawa, M. Matsuoka, S. Suzuki, A. Horino and T. Sasaki, *Journal of medical microbiology*, 2008, **57**, 469-475.
26. D. C. Krause, D. K. Leith, R. M. Wilson and J. B. Baseman, *Infection and immunity*, 1982, **35**, 809-817.
27. S. F. Dallo, A. L. Lazzell, A. Chavoya, S. P. Reddy and J. B. Baseman, *Infect Immun*, 1996, **64**, 2595-2601.

28. J. G. Tully, D. L. Rose, R. F. Whitcomb and R. P. Wenzel, *J Infect Dis*, 1979, **139**, 478-482.
29. N. L. Somerson, J. P. Kocka, D. Rose and R. A. Delgiudice, *Appl Environ Microb*, 1982, **43**, 412-417.
30. C. E. Romero-Arroyo, J. Jordan, S. J. Peacock, M. J. Willby, M. A. Farmer and D. C. Krause, *J Bacteriol*, 1999, **181**, 1079-1087.
31. S. Razin, *Biologicals*, 2010, **38**, 191-192.
32. S. Razin and L. Hayflick, *Biologicals*, 2010, **38**, 183-190.
33. S. P. Collins, R. K. Pope, R. W. Scheetz, R. I. Ray, P. A. Wagner and B. J. Little, *Microsc Res Techniq*, 1993, **25**, 398-405.
34. J. D. Mendelsohn, C. J. Barrett, V. V. Chan, A. J. Pal, A. M. Mayes and M. F. Rubner, *Langmuir*, 2000, **16**, 5017-5023.
35. P. Lavalle, C. Gergely, F. J. G. Cuisinier, G. Decher, P. Schaaf, J. C. Voegel and C. Picart, *Macromolecules*, 2002, **35**, 4458-4465.
36. L. L. Han, Z. W. Mao, J. D. Wu, Y. Guo, T. C. Ren and C. Y. Gao, *Biomaterials*, 2013, **34**, 975-984.
37. N. G. Veerabadran, P. L. Goli, S. S. Stewart-Clark, Y. M. Lvov and D. K. Mills, *Macromol Biosci*, 2007, **7**, 877-882.
38. J. Kapuscinski and W. Szer, *Nucleic acids research*, 1979, **6**, 3519-3534.
39. J. Kapuscinski and K. Yanagi, *Nucleic acids research*, 1979, **6**, 3535-3542.
40. I. Estrela-Lopis, S. Leporatti, S. Moya, A. Brandt, E. Donath and H. Mohwald, *Langmuir*, 2002, **18**, 7861-7866.
41. M. Ocwieja, Z. Adamczyk, M. Morga and A. Michna, *Journal of colloid and interface science*, 2011, **364**, 39-48.
42. G. J. Puppels, F. F. de Mul, C. Otto, J. Greve, M. Robert-Nicoud, D. J. Arndt-Jovin and T. M. Jovin, *Nature*, 1990, **347**, 301-303.
43. X. N. Lu, Q. Huang, W. G. Miller, D. E. Aston, J. Xu, F. Xue, H. W. Zhang, B. A. Rasco, S. Wang and M. E. Konkel, *J Clin Microbiol*, 2012, **50**, 2932-2946.
44. W. R. Premasiri, D. T. Moir, M. S. Klempner, N. Krieger, G. Jones, 2nd and L. D. Ziegler, *The journal of physical chemistry. B*, 2005, **109**, 312-320.
45. M. Kahraman, M. M. Yazici, F. Sahin, O. F. Bayrak and M. Culha, *Appl Spectrosc*, 2007, **61**, 479-485.
46. I. S. Patel, W. R. Premasiri, D. T. Moir and L. D. Ziegler, *Journal of Raman spectroscopy : JRS*, 2008, **39**, 1660-1672.
47. K. Maquelin, C. Kirschner, L. P. Choo-Smith, N. van den Braak, H. P. Endtz, D. Naumann and G. J. Puppels, *J Microbiol Meth*, 2002, **51**, 255-271.
48. L. J. Goeller and M. R. Riley, *Appl Spectrosc*, 2007, **61**, 679-685.
49. H. Y. Chu, Y. W. Huang and Y. P. Zhao, *Appl Spectrosc*, 2008, **62**, 922-931.
50. R. M. Jarvis and R. Goodacre, *Chem Soc Rev*, 2008, **37**, 931-936.
51. P. Negri, A. Kage, A. Nitsche, D. Naumann and R. A. Dluhy, *Chemical communications*, 2011, **47**, 8635-8637.
52. P. Negri, G. J. Chen, A. Kage, A. Nitsche, D. Naumann, B. Q. Xu and R. A. Dluhy, *Anal Chem*, 2012, **84**, 5501-5508.
53. S. L. Hennigan, J. D. Driskell, N. Ferguson-Noel, R. A. Dluhy, Y. P. Zhao, R. A. Tripp and D. C. Krause, *Appl Environ Microb*, 2012, **78**, 1930-1935.

54. A. Sengupta, M. Mujacic and E. J. Davis, *Analytical and bioanalytical chemistry*, 2006, **386**, 1379-1386.
55. M. Barker and W. Rayens, *J Chemometr*, 2003, **17**, 166-173.
56. G. Musumarra, V. Barresi, D. F. Condorelli, C. G. Fortuna and S. Scire, *J Chemometr*, 2004, **18**, 125-132.
57. J. W. Dorigo-Zetsma, S. A. Zaat, P. M. Wertheim-van Dillen, L. Spanjaard, J. Rijntjes, G. van Waveren, J. S. Jensen, A. F. Angulo and J. Dankert, *Journal of clinical microbiology*, 1999, **37**, 14-17.

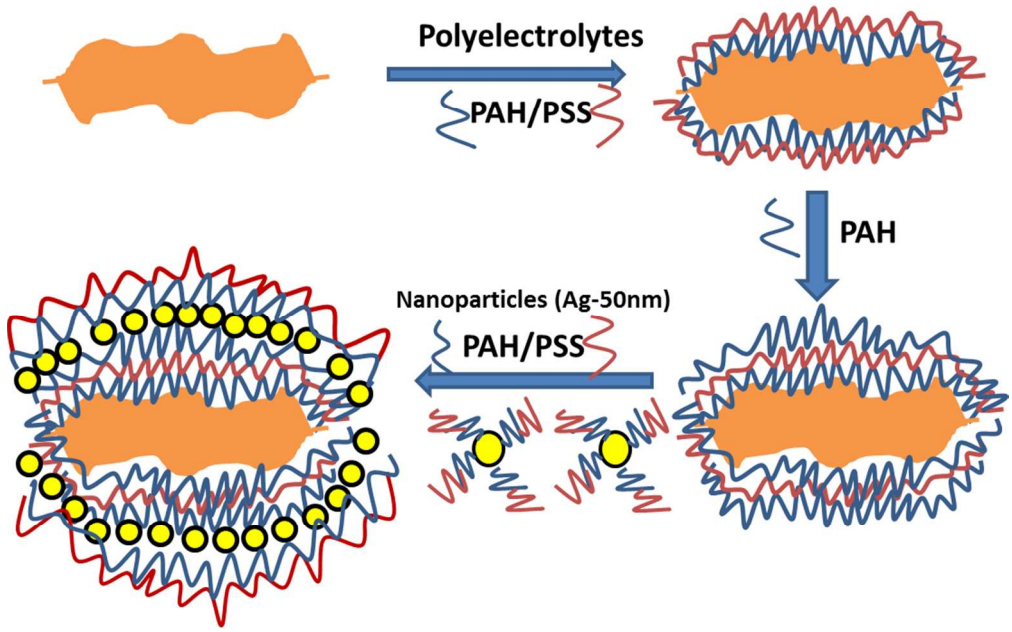

187x117mm (150 x 150 DPI)

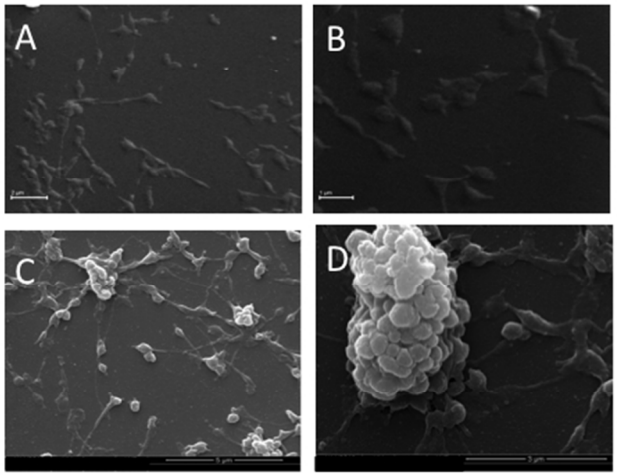

Figure 2

254x190mm (72 x 72 DPI)

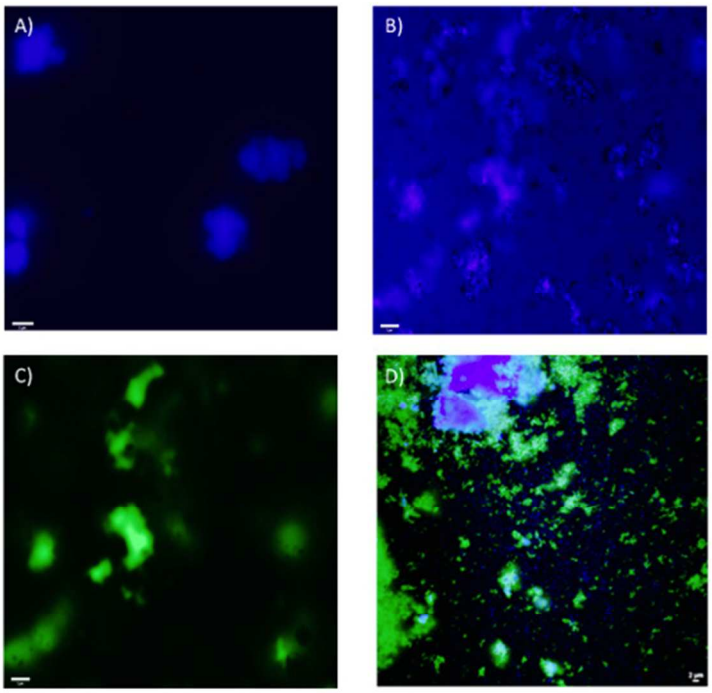

Figure 3

254x190mm (72 x 72 DPI)

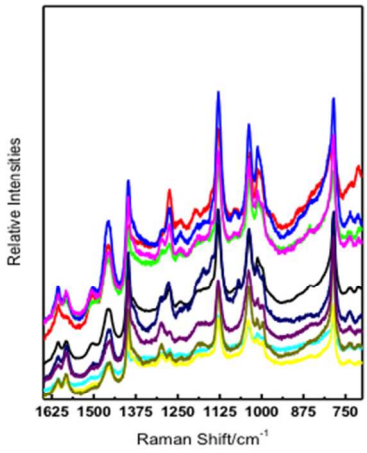

Figure 4

254x190mm (72 x 72 DPI)

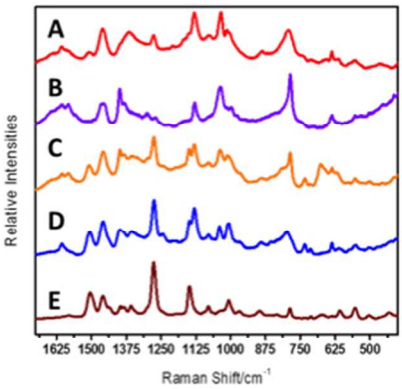

Figure 5

254x190mm (72 x 72 DPI)

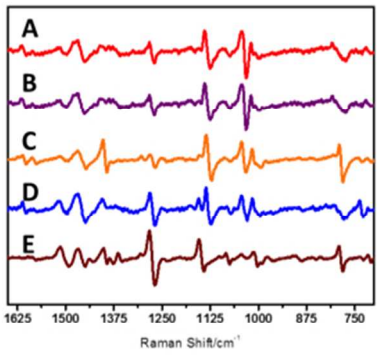

Figure 6

254x190mm (72 x 72 DPI)

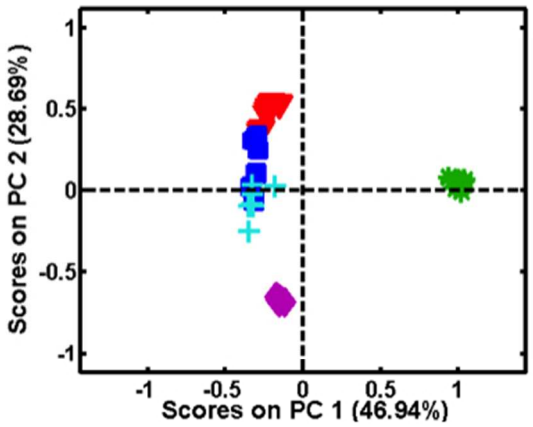

Figure 7

254x190mm (72 x 72 DPI)

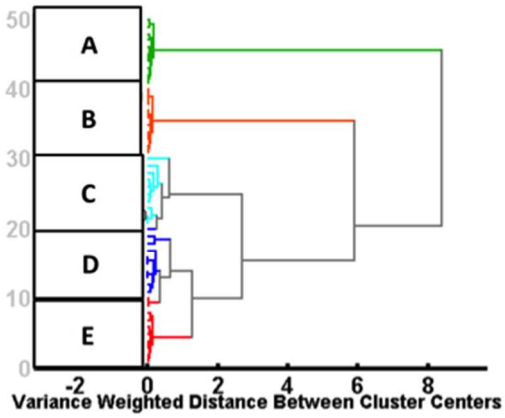

Figure 8

254x190mm (72 x 72 DPI)

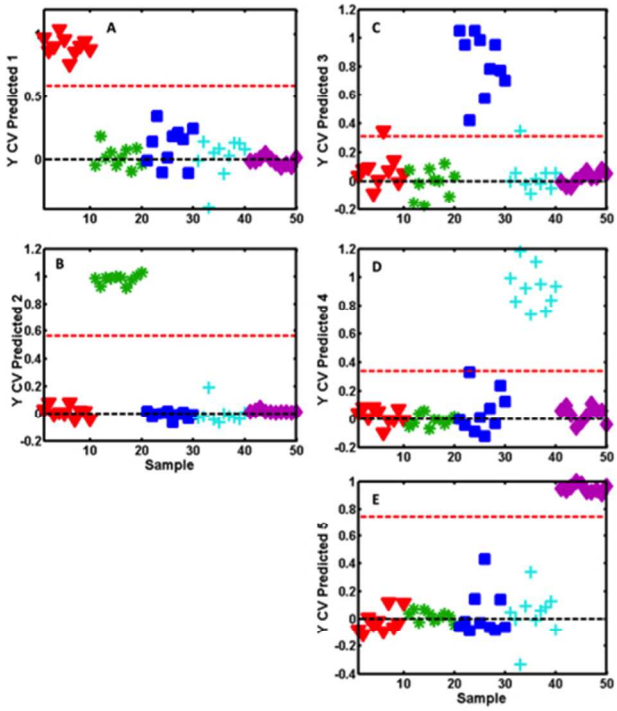

Figure 9

254x190mm (72 x 72 DPI)

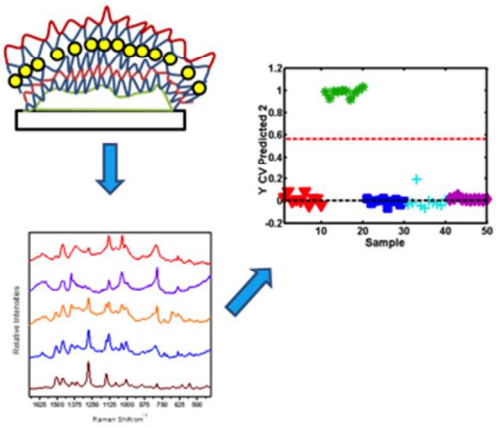

Graphical Abstract

254x190mm (72 x 72 DPI)